FLUX IDENTIFICATION FOR SCALAR CONSERVATION LAWS MODELLING SEDIMENTATION IN VESSELS WITH VARYING CROSS-SECTIONAL AREA

RAIMUND BÜRGER[A], JULIO CAREAGA[B], AND STEFAN DIEHL[C]

ABSTRACT. A method is presented for the identification of a non-convex flux function of a hyperbolic scalar conservation law that models sedimentation of solid particles in a liquid. While all previous identification methods are based on data obtained from settling tests in cylindrical vessels, the novel approach is based on the richer solution behaviour produced in a vessel with downward-decreasing cross-sectional area. Except for the initial homogeneous concentration, the data given for the present inverse problem are the location of the decline of the supernatant-suspension interface as a function of time. The inverse problem is solved by utilizing the construction of solutions of the direct problem by the method of characteristics. In theory, the entire flux function can be estimated from only one batch-settling experiment, and the solution is given by parametric and explicit formulas for the flux function. The method is tested on synthetic data (for example, generated by numerical simulations with a known flux) and on published experimental data.

1. INTRODUCTION

1.1. **Scope.** We are interested in the identification of the nonlinear flux function $f(\phi) = v(\phi)\phi$ appearing in a conservation law of the form

$$\frac{\partial \phi}{\partial t} - \frac{\partial f(\phi)}{\partial x} = 0, \tag{1.1}$$

where t is time and x the spatial coordinate. The partial differential equation (PDE) (1.1) arises as continuum model of diverse phenomena such as two-phase flow and traffic flow. The focus here is on sedimentation of small particles in a liquid, where ϕ is the volume fraction of the solids and v the (normalized) velocity of the solid phase. This velocity is given by some nonlinear constitutive function depending on the suspension under study; e.g. [11, 25, 31, 36, 41]. The solution of a hyperbolic equation like (1.1) along with initial data generally contains discontinuities (shock waves and contact discontinuities). By solving the inverse problem, we

Date: December 11, 2016.

Key words and phrases. batch sedimentation, explicit representation, inverse problem, nonlinear hyperbolic partial differential equation.

[A]CI^{2}MA and Departamento de Ingeniería Matemática, Facultad de Ciencias Físicas y Matemáticas, Universidad de Concepción, Casilla 160-C, Concepción, Chile. E-Mail: rburger@ing-mat.udec.cl.

[B]CI^{2}MA and Departamento de Ingeniería Matemática, Facultad de Ciencias Físicas y Matemáticas, Universidad de Concepción, Casilla 160-C, Concepción, Chile. E-Mail: juliocareaga@udec.cl.

[C]Centre for Mathematical Sciences, Lund University, P.O. Box 118, S-221 00 Lund, Sweden. E-Mail: diehl@maths.lth.se (corresponding author).

mean determining the constitutive function $v(\phi)$, or equivalently, the flux function $f(\phi)$, by observing the solution $\phi(x,t)$ of (1.1) or, as is the topic of this work, a slightly more complicated equation.

In applications, practical circumstances lay constraints on the mathematical formulation of a suitable inverse problem, which is often ill-conditioned or ill-posed, unless one or several sufficiently varied solutions of the direct problem are available and can be measured accurately. In the industrial process of continuous sedimentation of suspensions in mineral processing and wastewater treatment, the material properties vary with time and simple tests for identification need to be made regularly. There are many publications on controlled batch sedimentation experiments and the identification of the flux function; see Section 1.2. All of these consider a vessel with a constant cross-sectional area. We here present a novel identification method motivated by the following background. Inspired by the work of Anestis [1], we solved in [6] the batch sedimentation problem for a vessel where the cross-sectional area $A(x)$ increases with height x. In dimensionless variables, the direct problem is the following, where $x = 0$ is the bottom of the vessel:

$$\frac{\partial}{\partial t}\big(A(x)\phi\big) - \frac{\partial}{\partial x}\big(A(x)f(\phi)\big) = 0 \qquad \text{for } 0 < x < 1,\ t > 0, \tag{1.2a}$$

$$\phi(x,0) = \phi_0 \qquad \text{for } 0 < x < 1, \tag{1.2b}$$

$$\phi(0^+,t) = \phi_{\max} \quad \text{and} \quad \phi(1^-,t) = 0 \quad \text{for } t > 0. \tag{1.2c}$$

This model captures the hindered settling phenomenon where the particles settle and liquid is squeezed upwards. The widely used constitutive assumption by Kynch [34] states that the hindered settling velocity is a function of the local concentration ϕ only; $v = v(\phi) \geq 0$. The flux function $f(\phi) = v(\phi)\phi$ is assumed to have one inflection point $\phi_{\mathrm{infl}} \in (0, \phi_{\max})$, where $\phi_{\max}$ is the maximum packing concentration at which $v(\phi_{\max}) = 0$. The solution of (1.2) has a discontinuity $x = h(t)$ separating clear liquid above from the suspension below. Since this interface is clearly visible, its movement is easily captured. The inverse problem can be formulated as follows:

> *Given $\phi_0 > 0$ and the interface trajectory $[t_{\mathrm{start}}, t_{\mathrm{end}}] \ni t \mapsto h(t)$, find the portion of the flux function $\phi \mapsto f(\phi)$ corresponding to the interval of ϕ-values adjacent to that trajectory.* (IP)

The ϕ-values of the solution of (1.2) adjacent to the interface are not known; however, we utilize that they increase with time from ϕ_0 already from $t = 0$. The solution of (IP) is a parametric formula for a portion of f, which depends on ϕ_0, h and h'. Starting from measured data, one has to fit a height function $\bar{h}$ to the data, and the estimated flux $\bar{f}$ depends on $\bar{h}$ and its derivative. The solution of (IP) can also be given by an explicit flux function; however, there is a restriction on the fitting function to the (transformed) data; for example, a function made up of piecewise cubic polynomials works. In the case of a vessel with vertex at the bottom $x = 0$, the flux $f(\phi)$ can be identified for all $\phi \in [\phi_0, \phi_{\max}]$. This is much more than what can be obtained from a standard batch test in a cylindrical vessel. In that case, at most the flux values of $\{\phi_0\} \cup [\phi_0^*, \phi_{\max}]$ can be obtained, where $\phi_0^* > \phi_{\mathrm{infl}}$; see [8, 18, 34]. This advantage of settling in a vessel with $A' > 0$ is also illustrated in Figure 1. In other words, the solution of (1.2) is richer when $A' > 0$ than when $A' \equiv 0$. In the case that f has the unfavourable property that the solution of (1.2) contains a discontinuity created initially from the bottom and

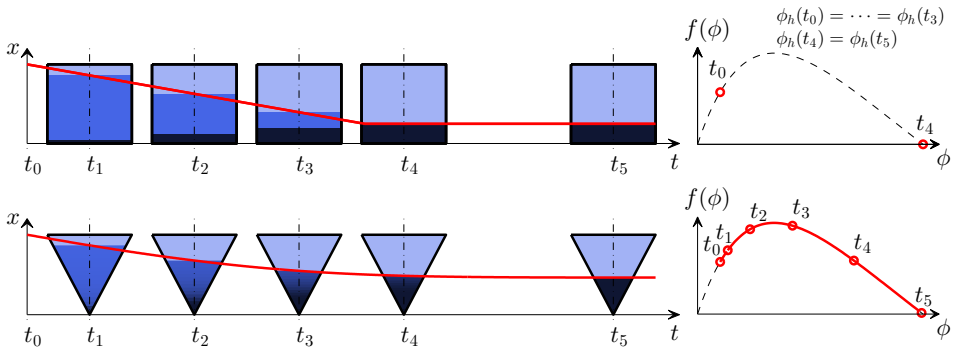

FIGURE 1. Schematic illustration (obtained from numerical simulations) of the information provided by the trajectory of the suspension-supernate interface for settling in a cylinder (top) and in a cone (bottom). The volume fraction just below the interface $x = h(t)$ is denoted by $\phi_h(t)$. In the cylindrical case shown, only the pairs $(\phi_0, f(\phi_0))$ and $(\phi_{\max}, f(\phi_{\max}))$ are involved, where ϕ_0 and $\phi_{\max}$ are the initial and maximum concentration, respectively. Under appropriate conditions, the (curved) trajectory in the conical case provides information on the portion of the flux plot marked in red, where $\phi_h(t_i)$ denotes the ϕ-value adjacent to the trajectory at $t = t_i$, $i = 1, \ldots, 5$.

which intersects the upper one $x = h(t)$, then f cannot be identified all the way up to $\phi_{\max}$. In such a case, an additional settling test in a cylindrical vessel ($A' \equiv 0$) can yield $f(\phi)$ for an interval $[\phi_0^*, \phi_{\max}]$, where $\phi_0^* > \phi_{\text{infl}}$; see [8].

Given discrete in time measurements of the discontinuity $x = h(t)$ in a vessel with a vertex at the bottom, we show how these are used in a quadratic programming problem, whose solution is substituted into an explicit formula for the identified portion of the flux function.

Conical vessels are frequently used both for laboratory sedimentation tests [5, 37, 40, 43, 45] and as industrial deep cone thickeners [24, 30, 44, 46].

1.2. **Related work.** Inverse problems for scalar conservation laws of type (1.1) (i.e. $A' \equiv 0$), where (a portion of) the flux function f is identified without any assumed parametric form, have been handled in various ways.

James and Sepúlveda [29] minimize a nonstandard cost functional containing the difference between observed data and the solution of (1.1) at a fixed time point. This is done via an adjoint equation obtained from a formal computation of the gradient of the cost function, although the latter may not be differentiable. Although the nonuniqueness of identifying f when the direct problem contains discontinuities is still an unresolved issue, the method has been used with some success in the application to sedimentation [3, 12].

Kang and Tanuma [32] assume that f is convex and that the initial data are such that a single shock wave is formed for large times. The latter is true for our batch sedimentation problem, but f often has (at least) one inflection point. Fernández-Berdaguer and Savioli [23, 42] identify the flux function via a least-squares technique

in functional spaces. However, they need to start with a continuous solution of the direct problem for small times, which is not the case in batch sedimentation. Castro and Zuazua [9] formulate the identification problem as an optimal control problem, prove the existence of minimizers and introduce an optimization strategy to obtain a numerical approximate flux also when the solution of the direct problem contains discontinuities.

The approach by Holden et al. [26] is based on the explicit construction of approximate solutions of the scalar equation $u_t+(k(x)f(u))_x = 0$ by the front tracking method [27]. The cases dealt with are when $k \equiv 1$ and f is identified and when f is known and a piecewise constant function $k(x)$ is identified. The latter case has applications in traffic flow, for example, finding a discontinuity of $k(x)$ corresponds to detecting where in a tunnel an accident has occurred by observing the density of traffic at both tunnel ends. In their other case when f is unknown, many solutions need to be observed, each having a finite number of simple shock or rarefaction waves due to suitably chosen initial data. The result is a continuous and piecewise affine approximate function of f. Their methods are difficult to apply to the problem of sedimentation; partly because many experiments have to be performed and partly since it is required that each initial data contain a specific discontinuity.

The identification method presented in [21] also produces a piecewise affine approximate flux function f given lots of accurate data points in time and space of the concentration from one experiment (i.e., one initial datum) [17].

For the specific problem of determining the flux function of gravity sedimentation from laboratory batch tests in cylindrical vessels, various methods have been presented. The most common one is to perform several standard batch settling experiments, each with a constant initial datum ϕ_0. If $\phi_0 < \phi_{\mathrm{infl}}$, then the upper discontinuity declines initially along a straight line with the velocity $v(\phi_0)$, and hence one point of the flux, $f(\phi_0) = v(\phi_0)\phi_0$ is obtained; e.g. [14, 16, 28, 33, 35].

The early graphical method by Kynch [34], where the flux function can be identified in an interval $[\phi_0^*, \phi_{\max}]$ of high concentrations above the inflection point of f, has been used widely. The graphical method was put in explicit formulas for f in [18] and developed to an advanced identification method in [8], and we refer to those papers for more references on the graphical method and other treatments with formulas. An experimental method for determining other parts of f based on fluidization was advanced in [38]. To estimate the concave part of the flux function including its maximum, a new experiment, where the initial data contain a discontinuity, was introduced in [18]. The methodology was further developed in [4, 8].

During a standard batch sedimentation experiment, only a subset of the volume fractions are present – at most $\{\phi_0\} \cup [\phi_0^*, \phi_{\max}]$. However, other parts of the flux function are important during transient behaviour in the industrial continuously operated clarifier-thickener units mentioned above. For the simulation and control of such processes, the part of the flux function including the maximum point is of importance; see [19, 20, 22].

1.3. **Outline of the paper.** The direct problem is treated in Section 2 where properties needed to solve (IP) are described. The assumptions behind the formulation (1.2) are given in Section 2.1 and the properties of the solution in the case $p > 0$ are reviewed from [6] in Section 2.2. In Section 2.3, the solution of (1.2) in the special case $p = 0$ is given for the first time. The theoretical solution of (IP)

(when the function $t \mapsto h(t)$ is given) is expounded in Section 3 for the two cases that f is given in parametric form (Section 3.1) and, alternatively, as an explicit function (Section 3.2). An explicit expression for f in the special case of exponentially widening cross-sectional area ($p > 0$, $q = 0$) is given in Section 3.3. For given discrete data points as measurements of the function $t \mapsto h(t)$, the fitting of piecewise cubic polynomials to transformed data, so that the formula for the explicit solution can be used, is presented in Section 4. For ease of reference, the two variants of methods of identification are summarized in Section 5. Eventually, Section 6 contains examples with synthetic and experimental data, and some conclusions are collected in Section 7.

2. Sedimentation in a vessel with varying cross-sectional area: the direct problem

2.1. **Assumptions and non-dimensionalization.** The governing mass balance equation in dimensional form for the concentration of solids $C = C(\tilde{x}, \tilde{t})$ is, for time $\tilde{t}$ and height $\tilde{x}$,

$$\frac{\partial}{\partial \tilde{t}}\big(\tilde{A}(\tilde{x})C\big) - \frac{\partial}{\partial \tilde{x}}\big(\tilde{A}(\tilde{x})\tilde{f}(C)\big) = 0 \quad \text{for } 0 < \tilde{x} < H \text{ and } \tilde{t} > 0, \tag{2.1}$$

where H is the height of the suspension and $\tilde{A} \in C^1[0, H]$ is the cross-sectional area. The unknown is the concentration of solids $C = \phi\varrho_\mathrm{s}$, where ϕ is the solids volume fraction and ϱ_s the solids density, which is assumed to be constant. Hence, there exists a maximum volume fraction $\phi_\mathrm{max} \leq 1$. The solid-fluid flux function, also called drift flux or Kynch batch flux [34] can be written $\tilde{f}(C) = \tilde{f}(\phi\varrho_\mathrm{s}) = \tilde{v}(\phi)\phi\varrho_\mathrm{s}$ with $\tilde{v}(\phi) := v_\infty v(\phi)$, where v_∞ is the settling velocity of a single particle and $v(\phi)$ is a dimensionless constitutive function that satisfies $v(0) = 1$ and $v(\phi_\mathrm{max}) = 0$. Hence, $f(\phi) := v(\phi)\phi$ is the dimensionless flux function, which we assume is unimodal and satisfies $0 \leq f \in C^1[0, \phi_\mathrm{max}]$ and $f(0) = f(\phi_\mathrm{max}) = 0$. We let $\hat{\phi}$ denote the maximum point of f and assume that there exists at most one inflection point $\phi_\mathrm{infl} \in (\hat{\phi}, \phi_\mathrm{max}]$. Then $v(\phi) = f(\phi)/\phi$ satisfies $v'(\phi) < 0$ for $0 < \phi < \phi_\mathrm{max}$; see [6].

Defining the variables $x := \tilde{x}/H$, $t := \tilde{t}v_\infty/H$, and $A(x) := \tilde{A}(\tilde{x})/\tilde{A}(H)$, we get from (2.1) the dimensionless hyperbolic PDE (1.2a). In regions of the x-t-plane where the solution is smooth, (1.2a) can be written as

$$\frac{\partial \phi}{\partial t} - f'(\phi)\frac{\partial \phi}{\partial x} = \frac{A'(x)}{A(x)} f(\phi),$$

and one can use the method of characteristics (cf., e.g., [27]) to obtain the solution in regions where the solution is smooth.

We require that across each smooth curve of discontinuity $x = x_\mathrm{d}(t)$, the values $\phi^\pm := \phi(x_\mathrm{d}(t)^\pm, t)$ satisfy the jump condition (also known as Rankine-Hugoniot condition; and which is a consequence of the conservation of mass)

$$-x_\mathrm{d}'(t) = S(\phi^+, \phi^-) := \begin{cases} \big(f(\phi^+) - f(\phi^-)\big)/(\phi^+ - \phi^-) & \text{if } \phi^+ \neq \phi^-, \\ f'(\phi) & \text{if } \phi^+ = \phi^- =: \phi, \end{cases} \tag{2.2}$$

and the jump entropy condition

$$S(u, \phi_-) \geq S(\phi_+, \phi_-) \quad \text{for all } u \text{ between } \phi^+ \text{ and } \phi^-. \tag{2.3}$$

The solution of (1.2) exists and is unique [39].

The construction of solutions by the method of characteristics is based on the following operations [2, 10]:

$$\phi^* := \sup\left\{u > \phi : S(\phi, u) \le S(\phi, v)\ \forall v \in (\phi, u]\right\} \quad \text{for } \phi \in [0, \phi_{\text{infl}}],$$
$$\phi^{**} := \inf\left\{u < \phi : u^* = \phi\right\} \quad \text{for } \phi \in [\phi_{\text{infl}}, \phi_{\max}].$$

In [6], we solved problem (1.2) assuming that $A(x) > 0$ satisfies

$$\frac{A'(x)}{A(x)} = \frac{1}{p + qx}, \quad A(1) = 1 \quad \Leftrightarrow \quad A(x) = \left(\frac{p + qx}{p + q}\right)^{1/q} \quad \text{for } 0 \le x \le 1, \quad (2.4)$$

in the main case $p, q > 0$ and the limit case $p > 0$ and $q \to 0^+$. Since $A(x) > 0$, we thus have $A'(x) > 0$. The limit case of (2.4) as $q \to 0^+$ is $A(x) = \mathrm{e}^{(x-1)/p}$, since $(1 + qx/p)^{1/q} \to \mathrm{e}^{x/p}$. Hence, the well-known case of a constant cross-sectional area ($A \equiv 1$) is obtained for $q = 0$ and $p \to \infty$. On the other hand, for $p > 0$, we can let $q \to \infty$ in (2.4) to also obtain $A(x) \to 1$. The particular value $q = 1/2$ means that $A(x)$ grows quadratically with the height x, i.e., the radius grows affinely, so that the vessel is part of a cone. A vessel with a vertex corresponds to $p = 0$.

In dimensional variables, the area functions are

$$\tilde{A}(\tilde{x}) = \begin{cases} \tilde{A}(H)\left(\dfrac{p + q\tilde{x}/H}{p + q}\right)^{1/q} & \text{if } p \ge 0,\ q > 0, \\ \tilde{A}(H)\mathrm{e}^{(\tilde{x}-H)/(pH)} & \text{if } p > 0 \text{ and } q = 0. \end{cases} \quad (2.5)$$

In the case $q > 0$ we have

$$\tilde{A}(0) = \tilde{A}(H)\left(\frac{p}{p + q}\right)^{1/q} \quad \Leftrightarrow \quad p = \frac{q\tilde{A}(0)^q}{\tilde{A}(H)^q - \tilde{A}(0)^q}.$$

Hence, $p = 0$ is equivalent to $\tilde{A}(0) = 0$, which means that the vessel has a vertex at the bottom $x = 0$. This case is included for the direct problem in Section 2.3 and for (IP) in Section 3. Note that the factor $\tilde{A}(H)$ in (2.5) does not influence the solution of (1.2). Hence, the only measurement needed of a vessel with a vertex at $x = 0$ (i.e., the case $p = 0$) is its height H.

The solutions described below and shown in Figures 2–4 are computed with the flux function

$$f(\phi) = \phi(\mathrm{e}^{-r_{\mathrm{V}}\phi} - \mathrm{e}^{-r_{\mathrm{V}}\phi_{\max}}), \quad (2.6)$$

where r_{V} is a parameter. (We have for simplicity skipped the constant $1/(1 - \mathrm{e}^{-r_{\mathrm{V}}\phi_{\max}})$ that implies $v(0) = 1$.)

2.2. **Properties of solutions of** (1.2) **in the case** $p > 0$**.** We here review some facts of the solutions of (1.2) from [6], where all details can be found. There are qualitatively different solutions depending on the initial value ϕ_0 in relation to properties of the flux function f. For a given f, three main cases can be distinguished: Case L if $\phi_0 \in (0, \phi^{**}_{\max}]$, Case M if $\phi_0 \in (\phi^{**}_{\max}, \phi_{\text{infl}})$ and Case H if $\phi_0 \in [\phi_{\text{infl}}, \phi_{\max})$. Figure 2 shows the solution in Case M, which has the richest structure of the three cases, with the presence of two discontinuities $x = h(t)$, $t > 0$, and $x = b(t)$, $0 < t < t_2$. In region I, the solution is defined by characteristics from the initial datum. This region exists up to the time point $t_{2.5}$. In regions IIa and IIb, the characteristics are all concave and emanate from the bottom discontinuity and the origin, respectively. Near the origin $(x, t) = (0, 0)$, there is a time point t_1

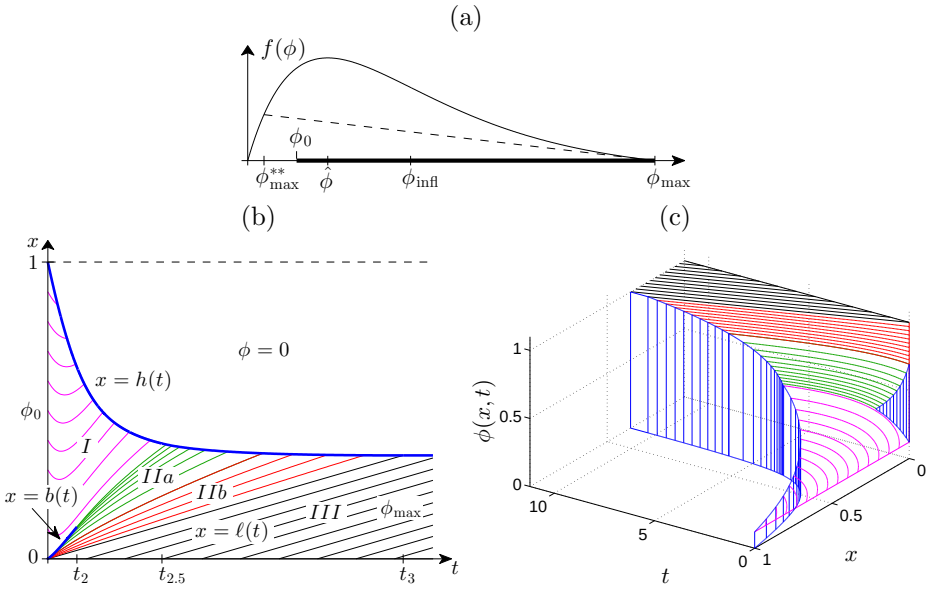

FIGURE 2. (a) Graph of the flux function (2.6) with $r_{\mathrm{V}} = 5$, $\phi_{\max} = 1$, $\phi^{**}_{\max} = 0.0398$, $\hat\phi = 0.196$ and $\phi_{\inf l} = 0.4$. Solution of (1.2) shown in 2D (b) and 3D (c) in a conical vessel with $p = 1/6$, $q = 1/2$, initial value $\phi_0 = 0.12$. Characteristics are shown by thin curves (except for the vertical blue lines representing the discontinuities in the 3D plot).

(not marked in the figure) before which the bottom discontinuity is a shock wave (characteristics enter it from both sides with positive angles) and after which it is a contact discontinuity (characteristics are tangential at least on one side). This local feature of the solution is however not essential for the inverse problem. The time point $t_3 := \sup\{t > 0 : \phi_h(t) < \phi_{\max}\}$ is finite if and only if $f'(\phi_{\max}) < 0$, which is the case shown in Figure 2 (a). Then $t_3 < \infty$ holds and the solution for $t \geq t_3$ consists of the two steady states $\phi = 0$ and $\phi = \phi_{\max}$ above and below $x = h(t_3)$, respectively. If $f'(\phi_{\max}) = 0$, then region III is empty.

We denote the solution values along the discontinuities by

$$\phi_h(t) := \phi\big(h(t)^-, t\big), \quad \phi_b(t) := \phi\big(b(t)^+, t\big) \quad \text{and} \quad \phi_b^-(t) := \phi\big(b(t)^-, t\big),$$

and define the following functions for $0 < \phi < \phi_{\max}$:

$$I(\phi) = I(\phi;\phi_0) := \int_{\phi_0}^{\phi} \frac{\mathrm{d}\Phi}{f(\Phi)^{1+q}},$$

$$Q(\phi) := f(\phi)^q I(\phi), \quad P(\phi) := f'(\phi) I(\phi) + \frac{1}{q f(\phi)^q}.$$

If $0 < \phi_0 \leq \phi_{\inf l}$ and $q > 0$, we also define

$$G(\varphi) := S(\varphi, \varphi^-) + \frac{1}{qQ(\varphi)}, \quad \varphi \in (\phi_0, \phi_{\inf l}], \tag{2.7}$$

where φ and $\varphi^- := \varphi^-(\varphi)$ satisfy the entropy condition (2.3).

The following lemma and theorem are proved in [6].

Lemma 2.1. *If $q = 0$, then $Q'(\phi) > 0$ for $\phi \in [\phi_0, \phi_{\max})$. Assume that $q > 0$.*

(i) *If $\phi_0 \geq \phi_{\mathrm{infl}}$ (Case H), then $P(\phi_{\mathrm{infl}}) > 0$ and $Q'(\phi) > 0$ for $\phi \in (\phi_0, \phi_{\max})$.*

(ii) *If $\phi_0 < \phi_{\mathrm{infl}}$ (Case L or M), then either $P(\phi_{\mathrm{infl}}) > 0$ and $Q'(\phi) > 0$ for $\phi \in [\phi_0, \phi_{\max})$, or $P(\phi_{\mathrm{infl}}) \leq 0$ and the following holds: There exists a unique zero ϕ_{cr} of Q' (the ϕ-value of conglomerating characteristics) in the interval $(\max(\phi_0, \hat{\phi}), \phi_{\mathrm{infl}}]$ such that $Q'(\phi) > 0$ for $\phi \in [\phi_0, \phi_{\mathrm{cr}})$, and there exists a unique zero $\phi_G \in (\phi_0, \phi_{\mathrm{cr}})$ of G with $G(\phi) \gtrless 0 \Leftrightarrow \phi \lessgtr \phi_G$.*

Theorem 2.1. *Assume that $A(x)$ is given by (2.4) with $p, q > 0$ or $p > 0$ and $q \to 0^+$. Then the entropy solution $\phi = \phi(x,t)$ of (1.2) is piecewise smooth and has the following properties:*

(i) *The solution in region I is given by*

$$\phi(x,t) = Q^{-1}\big(\psi(x,t)\big), \quad \text{where} \quad \psi(x,t) := \frac{t}{p+qx}. \tag{2.8}$$

For $q > 0$, (2.8) is equivalent to

$$x = \frac{t}{qQ(\phi)} - \frac{p}{q}; \tag{2.9}$$

hence, ϕ is constant on straight lines in the x-t-plane which all intersect the x-axis at $x = -p/q < 0$.

(ii) *A shock wave $x = h(t)$, $0 \leq t \leq t_{2.5}$, originates from the top and satisfies*

$$h'(t) = -v(\phi_h(t)), \tag{2.10}$$

$$\phi_h(t) = Q^{-1}\big(\psi(h(t),t)\big), \tag{2.11}$$

$$\phi_h'(t) > 0, \quad h'(t) < 0, \quad h''(t) > 0. \tag{2.12}$$

(iii) *A discontinuity $x = b(t)$ rises from the bottom if and only if $0 < \phi_0 < \phi_{\mathrm{infl}}$ (Cases L or M). It satisfies $b'(t) > 0$ and $b''(t) > 0$ for $0 \leq t < t_2$. If $P(\phi_{\mathrm{infl}}) > 0$, then either $b(t)$ meets the upper discontinuity at $t = t_2$ with $\phi_b(t_2) \leq \phi_{\mathrm{infl}}$, or $b(t_2) < h(t_2)$ and the solution is continuous at $(x,t) = (b(t_2), t_2)$ and $\phi(x,t) = \phi_{\mathrm{infl}}$, i.e., the bottom discontinuity ceases to exist at time t_2. If $P(\phi_{\mathrm{infl}}) \leq 0$, then $x = b(t)$ meets the upper discontinuity at $t = t_2$, i.e., $b(t_2) = h(t_2)$, and there exists a constant ϕ_G such that $\phi_b(t) < \phi_G < \phi_{\mathrm{cr}}$ for $0 \leq t < t_2$.*

(iv) *Region IIa is empty if $\phi_{\mathrm{infl}} < \phi_0 < \phi_{\max}$ (Case H). Otherwise, the solution in region IIa satisfies $\phi > \phi_{\mathrm{infl}}$ and is described by strictly concave characteristics emanating tangentially from $x = b(t)$ for $t_1 \leq t \leq t_2$.*

(v) *Region IIb is empty if $\phi_0 \leq \phi_{\max}^{**}$ (Case L). Otherwise region IIb is filled with a fan of concave characteristics emanating from the origin $(x,t) = (0,0)$ with initial values in the interval $(\phi_0^*, \phi_{\max})$ if $\phi_{\max}^{**} < \phi_0 < \phi_{\mathrm{infl}}$ (Case M), and in $(\phi_0, \phi_{\max})$ if $\phi_{\mathrm{infl}} \leq \phi_0 < \phi_{\max}$ (Case H).*

2.3. **Properties of solutions of (1.2) in the case $p = 0$ and $q > 0$.** When $p = 0$, we have $A(0) = 0$, i.e., the vessel has a vertex at the bottom $x = 0$. This case is not covered in [6]; however, it is highly interesting for the inverse problem for the following theoretical reason (in addition to the practical one that full conical vessels are often used). In Section 3, we present a solution of (IP) corresponding to the part of the upper discontinuity $x = h(t)$ above region I; see Figure 2. We have no identification method for values of $\phi_h(t)$ arising after the endpoint $t_{2.5}$ of region I, unless $t_{2.5} = t_3$. The time point $t_{2.5}$ can be detected by a discontinuity of

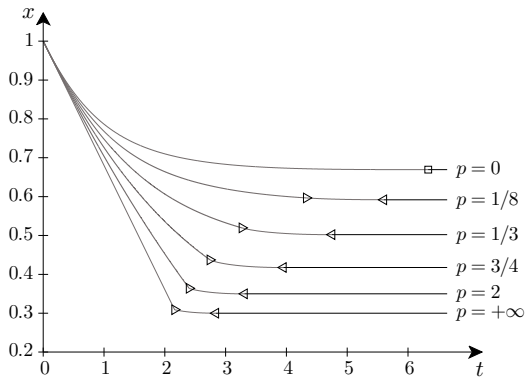

FIGURE 3. The upper discontinuity $x = h(t)$ for $q = 1/2$ and different values of p. The marked time points $t_{2.5}$ ($\triangleright$) and t_3 ($\triangleleft$) are different for $p > 0$ and coincide as $p = 0$ ($\square$).

h' in the case the bottom discontinuity $x = b(t)$ meets the upper one. Otherwise, h' is continuous at $t_{2.5}$ and this time point cannot be detected for general $p, q > 0$. However, as $p \to 0^+$, the time points $t_{2.5}$ and t_3 converge to the same value (proved below); see Figure 3.

Letting $p \to 0^+$ in the proof of Theorem 2.1 (which can be found in [6]) is not entirely straightforward. For $p > 0$, the solution $\phi(x, t)$ is continuous in a neighbourhood of the t-axis, except near $(x, t) = (0, 0)$ where a discontinuity can be created, having initially the volume fraction ϕ_0 above. As $p \to 0^+$, a singularity arises at the origin even if no discontinuity is created; all values of the interval $[\phi_0, \phi_{\max}]$ can be found in every neighbourhood of $(x, t) = (0, 0)$ so that the limit $\lim_{(x,t)\to(0,0)} \phi(x, t)$ (restricted to region I) does not exist. The volume fraction above a possible discontinuity depends on the properties of the flux f. The two subcases that may appear when $p = 0$ are shown in Figure 4 and given by the following theorem.

Theorem 2.2. *The entropy solution $\phi = \phi(x, t)$ of (1.2), where $A(x)$ is given by (2.4) with $p = 0$ and $q > 0$, is piecewise smooth and satisfies (i) and (ii) of Theorem 2.1. In particular, (2.8) gives that the solution in region I is constant on straight lines through the origin. If $f'(\phi_{\max}) < 0$, then $t_3 < \infty$ and the solution is constant $\phi \equiv \phi_{\max}$ in region III, which is bounded by the upper shock wave $x = h(t)$ and the line $x = \ell(t) := -f'(\phi_{\max})t$. If $f'(\phi_{\max}) = 0$, then region III is empty.*

(i) *(Cases L, M or H). If $P(\phi_{\text{infl}}) > 0$, then the solution is continuous in $0 \le x \le h(t)$, $t > 0$, and the line $x = \ell(t)$, $0 < t < t_3$, separates regions I and III; hence, $t_2 = t_{2.5} = t_3$.*

(ii) *(Cases L or M). If $P(\phi_{\text{infl}}) \le 0$, then there is a contact discontinuity $x = b(t)$, which is a straight line originating from the bottom, having the constant solution value ϕ_G above it, where ϕ_G is defined in Lemma 2.1 (ii). If $\phi_G < \phi^{**}$, then the value below $x = b(t)$ is $\phi_{\max}$ and region IIa is empty. Otherwise the value below $x = b(t)$ is ϕ_G^*. The discontinuity intersects $x = h(t)$ at $t = t_2 = t_{2.5}$. The jump in $\phi_h(t_2^-) = \phi_G$ up to $\phi_h(t_2^+) = \phi_G^*$*

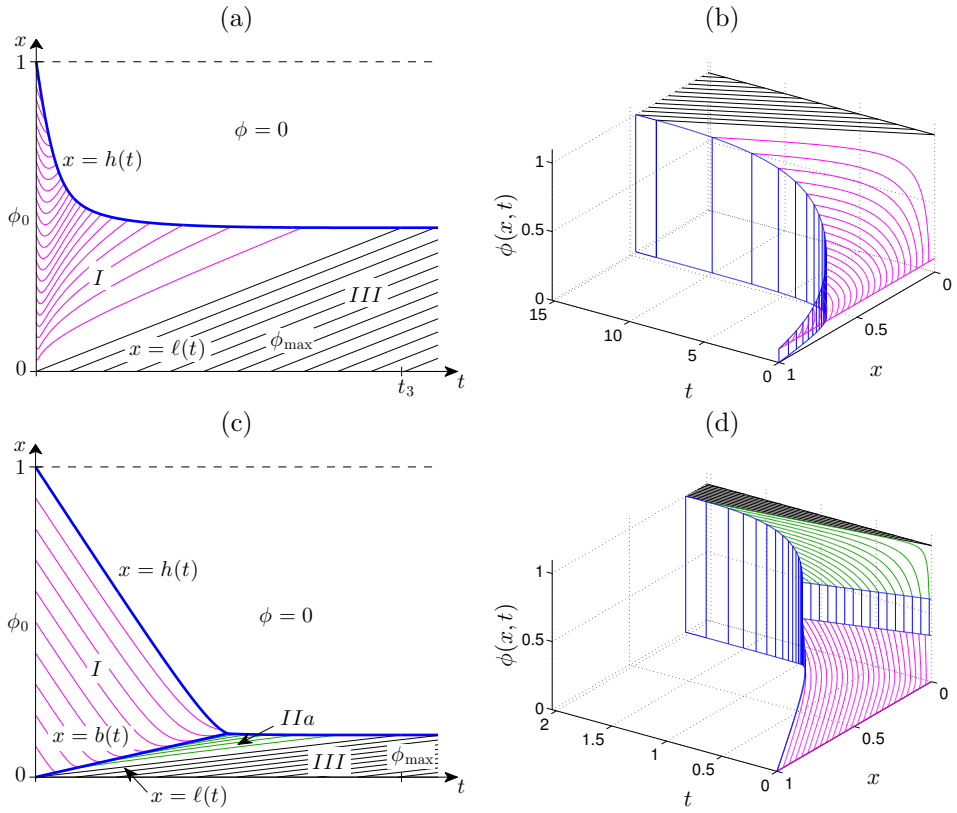

FIGURE 4. Solutions of (1.2) obtained by the method of characteristics for a full conical vessel with $p = 0$ and $q = 1/2$ in the two cases of Theorem 2.2. Case (i): Plots (a) and (b) show a continuous solution below $x = h(t)$ with $\phi_0 = 0.1$ (Case M). Case (ii): Plots (c) and (d) with two discontinuities with $\phi_0 = 0.0025$ (Case L).

implies a jump in $h'(t)$ at $t = t_2$. Furthermore, in region IIa, the solution of (1.2) *satisfies $\phi > \phi^*_G > \phi^*_{\mathrm{cr}} \geq \phi_{\mathrm{infl}}$ and is described by strictly concave characteristics emanating tangentially from the bottom discontinuity $x = b(t)$ for $0 \leq t \leq t_2$. Theorem 2.1 (v) holds in this subcase.*

Proof. Most of the statements are direct consequences of setting $p = 0$ in the proof of Theorem 2.1; see [6]. The new ingredient to prove in case (ii) is that the bottom discontinuity is a straight line with constant ϕ-values on both sides. For a curve $x = b(t)$, $b(0) = 0$, to satisfy both the jump and entropy conditions (2.2) and (2.3), and with the solution ϕ given by (2.8) in region I above it, the following ODE should be satisfied for $\phi_b(t)$ for $t > 0$; see Case L of [6]:

$$\phi_b'(t) = \frac{t}{Q'(\phi_b(t))qb(t)^2} G\big(\phi_b(t)\big).$$

This equation has $\phi_b(t) \equiv \phi_G$, $t > 0$, as a constant solution. We construct the entropy-satisfying solution by first defining the function

$$b(t) := \frac{t}{qQ(\phi_G)} = -S\big(\phi_G, \min(\phi_{\max}, \phi_G^*)\big)t, \tag{2.13}$$

where the last equality follows from the fact that ϕ_G is the zero of G; see (2.7). In region I, let the solution ϕ be given by (2.8) with $p = 0$ in the region $b(t) < x < h(t)$, $t > 0$. Just above $x = b(t)$, the solution ϕ is constant equal to ϕ_G by (2.9) (with $p = 0$). Letting $x = b(t)$ be a discontinuity with the value $\min(\phi_{\max}, \phi_G^*)$ just below, the entropy condition is satisfied by (2.13). If $\phi_G < \phi_{\max}^{**}$, then the solution is $\phi \equiv \phi_{\max}$ for $0 < x < b(t)$, $t > 0$, and region IIa is empty. Otherwise, $\phi \equiv \phi_G^*$ holds just below the line $x = b(t)$. At each point of this line, characteristics emanate tangentially defining the solution in region IIa as in the case of the proof of Theorem 2.1 (see [6]). □

3. Theoretical solution of the inverse problem

3.1. **Parametric formulas in the case $p \geq 0$ and $q > 0$.** The upper shock wave $x = h(t)$, $0 \leq t < t_{2.5}$, satisfies (2.10) and (2.11), where the latter can be written as

$$\psi\big(h(t), t\big) = f(\phi_h)^q I(\phi_h). \tag{3.1}$$

These two equations define the functions h and ϕ_h for given flux function f. Assume now that h and its derivative are known and let the two equations define ϕ_h and f. The following theorem states that a part of f can be obtained with an explicit parametrization.

Theorem 3.1. *Assume that $A(x)$ is given by (2.4) with $p \geq 0$ and $q > 0$, and that ϕ_0 and the upper shock wave $x = h(t)$, $0 \leq t < t_{2.5}$, are known. Then the inverse problem* (IP) *has the following parametrized solution:*

$$\big(\phi, f(\phi)\big) = \phi_0 \frac{(p+q)^{1+1/q}}{(p+qh(t))^{1/q}(p+q\eta(t))}\big(1, -h'(t)\big), \quad 0 \leq t \leq t_{2.5}, \tag{3.2}$$

where $\eta(t) := h(t) - th'(t)$.

Proof. The idea is to differentiate both (2.10) and (3.1) so that four equations are obtained. These are then used to get an equation without f and f', only ϕ_h, h and their derivatives should appear. First, (2.10) gives

$$f(\phi_h) = -h'\phi_h, \qquad f'(\phi_h)\phi_h' = -h''\phi_h - h'\phi_h'. \tag{3.3}$$

Differentiating (3.1), we get

$$\frac{\mathrm{d}}{\mathrm{d}t}\psi(h(t), t) = \big(qf(\phi_h)^q f'(\phi_h) I(\phi_h) + 1\big)\frac{\phi_h'}{f(\phi_h)}.$$

Inserting $I = \psi/f^q$ (from (3.1)) and using (3.3) to eliminate f and f' we get

$$\frac{\mathrm{d}}{\mathrm{d}t}\psi(h(t), t) = \left(q\psi(h,t)\left(-h''\frac{\phi_h}{\phi_h'} - h'\right) + 1\right)\frac{\phi_h'}{-h'\phi_h}.$$

This identity can be rewritten as follows:

$$\frac{\phi_h'}{\phi_h} = g(t), \quad \text{with} \quad g(t) := \frac{1}{qh'\psi(h,t) - 1}\left(h'\frac{\mathrm{d}}{\mathrm{d}t}\big(\psi(h,t)\big) - q\psi(h,t)h''\right), \tag{3.4}$$

where $q\psi(h,t)h' - 1 < 0$ since $h' < 0$. Defining the integral

$$\mathcal{G}(t) := \int_0^t g(s)\,\mathrm{d}s,$$

we may express the solution of (3.4) as $\phi_h = \phi_0 \exp(\mathcal{G}(t))$. Hence, by (3.3) a parametrized solution of (IP) can be written as

$$\big(\phi, f(\phi)\big) = \phi_0 \exp\big(\mathcal{G}(t)\big)\big(1, -h'(t)\big). \tag{3.5}$$

Since, by (2.12) and (3.4), $\mathcal{G}'(t) = g(t) = \phi_h'/\phi_h > 0$, the first component of (3.5) gives formally $t = \mathcal{G}^{-1}(\log(\phi/\phi_0))$ and hence the following formally explicit solution of the inverse problem:

$$f(\phi) = -\phi h'\left(\mathcal{G}^{-1}\left(\log\frac{\phi}{\phi_0}\right)\right), \quad \phi_0 \le \phi \le \phi_h(t_{2.5}). \tag{3.6}$$

We now compute $\mathcal{G}(t)$. Noting that

$$h'\frac{\mathrm{d}}{\mathrm{d}t}\big(\psi(h,t)\big) = \frac{\mathrm{d}}{\mathrm{d}t}\big(h'\psi(h,t)\big) - h''\psi(h,t),$$

we can write

$$g(t) = \frac{1}{1-qh'\psi(h,t)}\left(-\frac{\mathrm{d}}{\mathrm{d}t}\big(h'\psi(h,t)\big) + h''\psi(h,t) + qh''\psi(h,t)\right) =: g_1(t) + g_2(t),$$

where the first term can be written by means of $\eta(t) := h(t) - th'(t)$ as

$$g_1(t) = \frac{-(\mathrm{d}/\mathrm{d}t)(h'\psi(h,t))}{1-qh'\psi(h,t)} = \frac{1}{q}\frac{\mathrm{d}}{\mathrm{d}t}\log\big(1-qh'\psi(h,t)\big) = \frac{1}{q}\frac{\mathrm{d}}{\mathrm{d}t}\log\frac{p+q\eta(t)}{p+qh(t)}$$

and the second term as follows, by noting that $\eta'(t) = -th''(t)$:

$$g_2(t) = \frac{(1+q)h''\psi(h,t)}{1-qh'\psi(h,t)} = -(1+q)\frac{\eta'(t)}{p+q\eta(t)} = -\frac{1+q}{q}\frac{\mathrm{d}}{\mathrm{d}t}\log\big(p+q\eta(t)\big).$$

Hence, we get

$$\begin{aligned}\mathcal{G}(t) &= \int_0^t \big(g_1(s) + g_2(s)\big)\,\mathrm{d}s \\ &= \int_0^t \left(-\frac{1}{q}\frac{\mathrm{d}}{\mathrm{d}s}\log(p+qh(s)) - \frac{\mathrm{d}}{\mathrm{d}s}\log\big(p+q\eta(s)\big)\right)\mathrm{d}s \\ &= -\frac{1}{q}\log\frac{p+qh(t)}{p+q} - \log\frac{p+q\eta(t)}{p+q} = \log\frac{(p+q)^{1+1/q}}{(p+qh(t))^{1/q}(p+q\eta(t))}. \end{aligned} \tag{3.7}$$

Inserting this into (3.5) yields (3.2). □

Remark 3.1. *The special case when $A \equiv 1$ is obtained as $p > 0$ and $q \to \infty$, which is easiest calculated from* (3.7). *One gets $\mathcal{G}(t) \to -\log\eta(t)$, so that $\phi_h = \phi_0/\eta(t)$, which is in accordance with [8, 18]. In fact, when A is constant, the solution in the region corresponding to I and IIb is described by straight-line characteristics along which ϕ is constant. In region IIb they all intersect at the origin and form a rarefaction wave. In particular for region I, where $\phi \equiv \phi_0$ holds, we have by* (2.10) *for the upper shock wave: $-h'(t) = v(\phi_0)$, so that $\eta'(t) = -th''(t) = 0$. Hence, $\eta(t)$ is constant and $\eta(t) = \eta(0) = h(0) = 1$.*

3.2. **Explicit formulas in the case $p \geq 0$ and $q > 0$.** We will here derive an explicit representation of the flux function $f(\phi)$ for $\phi = \phi_h(t)$, $0 \leq t \leq t_{2.5}$ in terms of h and h'. The idea is to solve for t the first component of (3.2), which is

$$\phi = \frac{\phi_p}{(p+qh(t))^{1/q}\big(p+q\eta(t)\big)} \quad \text{where } \phi_p := \phi_0(p+q)^{1+1/q}, \tag{3.8}$$

and substitute the resulting expression of ϕ into the second component of (3.2). We first define and calculate

$$\begin{aligned} s(t) :=& \big(p+qh(t)\big)^{1+1/q}, \\ s'(t) =& (q+1)h'(t)\big(p+qh(t)\big)^{1/q}, \\ s''(t) =& (q+1)h''(t)\big(p+qh(t)\big)^{1/q} + (q+1)h'(t)^2\big(p+qh(t)\big)^{1/q-1}, \end{aligned} \tag{3.9}$$

and see that the following properties (cf. (2.12)) are carried over to s for $0 \leq t < t_{2.5}$:

$$h'(t) < 0, \quad h''(t) > 0 \quad \Leftrightarrow \quad s'(t) < 0, \quad s''(t) > 0. \tag{3.10}$$

The denominator of (3.8) can be written as

$$\begin{aligned} 0 < \big(p+qh(t)\big)^{1/q}\big(p+qh(t)-qth'(t)\big) &= \big(p+qh(t)\big)^{1/q+1} - qth'(t)\big(p+qh(t)\big)^{1/q} \\ &= s(t) - \frac{qt}{q+1}s'(t) =: \sigma(t). \end{aligned} \tag{3.11}$$

Since $\sigma'(t) = (s'(t) - qts''(t))/(q+1) < 0$ by (3.10), the inverse σ^{-1} of σ exists and we have proved the following theorem.

Theorem 3.2. *Assume that $A(x)$ is given by (2.4) with $p \geq 0$, $q > 0$, and that ϕ_0 and the upper shock wave $x = h(t)$, $0 \leq t < t_{2.5}$, are known. Then the inverse problem* (IP) *has the following explicit solution:*

$$f(\phi) = -\phi h'\left(\sigma^{-1}\left(\frac{\phi_p}{\phi}\right)\right), \quad \phi_0 \leq \phi \leq \phi_h(t_{2.5}), \tag{3.12}$$

where $s(t) := (p+qh(t))^{1/q+1}$ and $\sigma(t) := s(t) - qts'(t)/(q+1)$.

3.3. **The exponential case: $p > 0$ and $q = 0$.** This case means that the vessel has an exponentially increasing cross-sectional area $A(x) = \mathrm{e}^{(x-1)/p}$. We have $\psi = t/p$ and get from the proof of Theorem 3.1

$$\mathcal{G}(t) = -\int_0^t h'(s)\frac{1}{p}\,\mathrm{d}s = \frac{1-h(t)}{p}.$$

The function $\mathcal{G}$ is clearly invertible and we get the relation $\mathcal{G}^{-1}(y) = h^{-1}(1-py)$. Hence, (3.5) and (3.6) give both a parametric and an explicit representation:

$$\begin{aligned} \phi = \phi_0 \exp\left(\frac{1-h(t)}{p}\right) \quad &\Leftrightarrow \quad h(t) = 1 - p\log\frac{\phi}{\phi_0}, \\ f(\phi) = -\phi h'\left(h^{-1}\left(1-p\log\frac{\phi}{\phi_0}\right)\right)&. \end{aligned} \tag{3.13}$$

We remark that letting $p \to \infty$ we only get $\phi = \phi_0$, which is the solution in region I in the case of a constant cross-sectional area.

For an exponentially increasing area, it is thus possible to obtain an explicit representation of a portion of the flux function with (3.13) by fitting to data an

explicitly invertible function $\bar{h}$ that approximates h. The procedure for this is described in Section 4 for the common conical vessel shape ($q = 1/2$).

4. Solution of the inverse problem by curve fitting to data

4.1. **Fitting functions to data.** To use the explicit representation of f (3.12), one must be able to find an explicit expression for σ^{-1}; hence, we need a simple expression for σ that can be inverted. The corresponding function s can be obtained from the definition of σ (3.11); one gets, for some $t_0 > 0$,

$$s(t) = t^{1+1/q}\left(\frac{s(t_0)}{t_0^{1+1/q}} - \frac{q+1}{q}\int_{t_0}^{t}\frac{\sigma(\tau)}{\tau^{2+1/q}}\mathrm{d}\tau\right). \tag{4.1}$$

For example, letting $\sigma = \bar{\sigma}$ be a second-order polynomial, we obtain from (4.1)

$$\bar{s}(t) = c_3 t^{1+1/q} + c_2 t^2 + c_1 t + c_0 \tag{4.2}$$

for some constants c_i, $i = 0, \ldots, 3$. These constants can be determined by the given measured height data, i.e., one should fit the function, see (3.9),

$$\bar{h}(t) = \frac{1}{q}\big(\bar{s}(t)^{q/(q+1)} - p\big) = \frac{1}{q}\Big(\big(c_3 t^{1+1/q} + c_2 t^2 + c_1 t + c_0\big)^{q/(q+1)} - p\Big).$$

This is a nonlinear function of the coefficients. An alternative way is to first transform the height data h_i to $s_i = (p+qh_i)^{1+1/q}$ and directly determine the coefficients c_i, $i = 0, \ldots, 3$, which appear linearly in the expression (4.2) for $\bar{s}$. We will do the latter below. To demonstrate the method with simplified coefficients, we let $q = 1/2$ in the next subsection, which means that $\bar{s}$ is a cubic polynomial.

4.2. **Fitting piecewise cubic polynomials to transformed data.** For simplicity, we set in this section $q = 1/2$, which means that the vessel is a (truncated) cone. To use the explicit formula (3.12), we will approximate s by a function $\bar{s}$, which is obtained by a fit to correspondingly transformed data via (3.9), i.e., $s_i = (p + h_i/2)^3$, for each height data h_i. This is done by solving an optimization problem; see Section 4.3. Then we define $\bar{\sigma}(t) := \bar{s}(t) - t\bar{s}'(t)/3$, show that it has an explicit inverse and use (3.12) to obtain an estimation $\bar{f}$ of f. We will below represent $\bar{s}$ by piecewise highly regular functions with lower regularity at the fitting points. Similarly can be done for the parametric formula (3.8), which requires a fitted function $\bar{h}(t)$ directly to the data. The following theorem follows directly from (3.8) and (3.12).

Theorem 4.1. *If $\bar{s} \in C^k[0, t_{2.5}]$, for some $k \geq 2$, then the identified flux function defined by* (3.12) *satisfies $\bar{f} \in C^{k-1}[\phi_0, \phi_h(t_{2.5})]$. The analogue statement holds for* (3.8)*; $\bar{h} \in C^k[0, t_{2.5}]$ implies $\bar{f} \in C^{k-1}[\phi_0, \phi_h(t_{2.5})]$.*

Assume that we are given N pairs of data points that represent the curved discontinuity h in the interval $[0, t_{2.5}]$:

$$(t_j, x_j), \qquad j = 1, \ldots, j_2, \ldots, j_3, \ldots, j_n, \ldots, N. \tag{4.3}$$

Let $j_1 := 1$ and $j_{n+1} := N$. For each j the respective observed value of the s-curve is defined by

$$(t_j, z_j) := \big(t_j, (p + x_j/2)^3\big), \qquad j = 1, \ldots, j_2, \ldots, j_3, \ldots, j_n, \ldots, N. \tag{4.4}$$

The number of data points belonging to each interval $(t_{j_i}, t_{j_{i+1}}]$ is $N_i := j_{i+1} - j_i$, so that $N = 1 + \sum_{i=1}^{n} N_i$. We would like to fit smooth functions $\bar{s}_i$, $i = 1, \dots, n$ close to these data such that the graph of

$$\bar{s}(t) := \sum_{i=1}^{n} \bar{s}_i(t)\chi_i(t) \quad \text{for } t_1 < t \le t_N, \quad \text{where } \chi_i(t) = \begin{cases} 1 & \text{if } t_{j_i} < t \le t_{j_{i+1}}, \\ 0 & \text{otherwise,} \end{cases} \tag{4.5}$$

is an estimation of the curve s. The goal is to substitute (4.5) into (3.12) to obtain an explicit formula for a portion of the batch settling flux function $\bar{f}$. Then each function s_i should be chosen such that $\bar{\sigma}_i(t) := \bar{s}_i(t) - t\bar{s}_i'(t)/3$ is invertible explicitly. As was shown in Section 4.1, a cubic polynomial is suitable. We get

$$\begin{aligned} &\bar{s}_i(t) = a_i t^3 + b_i t^2 + c_i t + d_i, && \bar{s}_i'(t) = 3a_i t^2 + 2b_i t + c_i, \\ &\bar{s}_i''(t) = 6a_i t + 2b_i, && \bar{\sigma}_i(t) = \frac{b_i}{3} t^2 + \frac{2c_i}{3} t + d_i. \end{aligned}$$

Hence, each $\bar{\sigma}_i$ is a second-order polynomial. Note that exactly the same $\bar{\sigma}_i$ is obtained for a second-order polynomial $\bar{s}_i$ (set $a_i = 0$); hence, this is a worse alternative from a fitting point of view.

An explicit representation of the inverse of $\bar{\sigma}(t) := \bar{s}(t) - t\bar{s}'(t)/3$ requires some preparation. We have $\bar{s}_i \in C^\infty$, $i = 1, 2, \dots, n$, and to obtain $\bar{s} \in C^2[t_1, t_N]$ we impose the following continuity constraints at the fitting points:

$$\bar{s}_{i-1}(t_{j_i}) = \bar{s}_i(t_{j_i}), \quad i = 2, \dots, n, \tag{4.6}$$

$$\bar{s}_{i-1}'(t_{j_i}) = \bar{s}_i'(t_{j_i}), \quad i = 2, \dots, n, \tag{4.7}$$

$$\bar{s}_{i-1}''(t_{j_i}) = \bar{s}_i''(t_{j_i}), \quad i = 2, \dots, n. \tag{4.8}$$

These constitute $3(n-1)$ equations of the $4n$ parameters. To obtain a unique solution of a least-squares minimization problem (see Theorem 4.2 in Section 4.3), it turns out that in each interval $(t_{j_i}, t_{j_{i+1}}]$, there should be at least as many data points as parameters, i.e., $j_{i+1} - j_i \ge 4$, which implies that the total number N of data points should satisfy

$$N = j_{n+1} = 1 + \sum_{i=1}^{n} (j_{i+1} - j_i) \ge 1 + 4n.$$

In accordance with (3.10), we require

$$\bar{s}_i'(t) < 0, \qquad t_{j_i} \le t \le t_{j_{i+1}}, \quad i = 1, \dots, n, \tag{4.9}$$

$$\bar{s}_i''(t) = 6a_i t + 2b_i > 0, \quad t_{j_i} \le t \le t_{j_{i+1}}, \quad i = 1, \dots, n. \tag{4.10}$$

Because of the continuity constraint (4.7) and the convexity condition (4.10), we can conclude that $\bar{s}'$ is increasing. Hence, (4.9) can be replaced by the single constraint

$$\bar{s}_n'(t_N) = 3a_n t_N^2 + 2b_n t_N + c_n < 0. \tag{4.11}$$

To obtain simple constraints in the minimization problem, we assume that

$$a_i < 0 \quad \text{and} \quad b_i > 0, \quad i = 1, \dots, n. \tag{4.12}$$

Then all functions $s_i''(t)$ are decreasing. By virtue of the continuity constraints (4.8), we can replace all constraints (4.10) by the single one

$$\bar{s}_n''(t_N) = 6a_n t_N + 2b_n > 0. \tag{4.13}$$

Furthermore, we now get the same expression for the inverses of all σ_i. Since $\bar{\sigma}_i'(t) = 2s_i'(t)/3 - ts_i''(t)/3 < 0$ (by (3.10)), the left branch of the parabola should be used for the inverse, which is

$$\bar{\sigma}_i^{-1}(y) = -\frac{c_i + \sqrt{c_i^2 - 3b_i(d_i - y)}}{b_i}. \tag{4.14}$$

Hence, with $y = \phi_p/\phi$, $t = \bar{\sigma}_i^{-1}(y)$, $\bar{h}_i(t) := 2(\bar{s}_i^{1/3}(t) - p)$ and

$$\bar{h}_i'(t) = \frac{\mathrm{d}}{\mathrm{d}t} 2\big(\bar{s}_i(t)^{1/3} - p\big) = \frac{2\bar{s}_i'(t)}{3\bar{s}_i(t)^{2/3}} = \frac{2(3a_it^2 + 2b_it + c_i)}{3(a_it^3 + b_it^2 + c_it + d_i)^{2/3}}, \tag{4.15}$$

the explicit representation of $\bar{f}$, restricted to the values of ϕ corresponding to the interval $(t_{j_i}, t_{j_{i+1}}]$, is given by (3.12).

To obtain the estimation $\bar{f}$ corresponding to the entire interval $[\phi_0, \phi_h(t_{2.5})]$, we see that the continuity constraints (4.6)–(4.7) imply that, for $t_1 < t \le t_N$,

$$\bar{\sigma}(t) := \bar{s}(t) - \frac{t}{3}\bar{s}'(t) = \sum_{i=1}^{n} \left(\bar{s}_i(t) - \frac{t}{3}\bar{s}_i'(t) \right) \chi_i(t) = \sum_{i=1}^{n} \bar{\sigma}_i(t)\chi_i(t).$$

The inverse of $\bar{\sigma}$ can be written as a sum of the inverses of all $\bar{\sigma}_i$ by means of transformed characteristic functions χ_i. Since $\bar{\sigma}$ is decreasing, it maps the interval $(t_{j_i}, t_{j_{i+1}}]$ to the interval $[\bar{\sigma}(t_{j_{i+1}}), \bar{\sigma}(t_{j_i}))$. Because of the argument of σ^{-1} in (3.12), the corresponding interval for ϕ is

$$\bar{\sigma}(t_{j_{i+1}}) \le \frac{\phi_p}{\phi} < \bar{\sigma}(t_{j_i}) \quad \Leftrightarrow \quad \frac{\phi_p}{\bar{\sigma}(t_{j_i})} < \phi \le \frac{\phi_p}{\bar{\sigma}(t_{j_{i+1}})}.$$

Consequently, to express the inverse of $\bar{\sigma}$ we define the characteristic functions

$$\zeta_i(\phi) = \begin{cases} 1 & \text{if } \dfrac{\phi_p}{\bar{\sigma}(t_{j_i})} < \phi \le \dfrac{\phi_p}{\bar{\sigma}(t_{j_{i+1}})}, \\ 0 & \text{otherwise,} \end{cases} \qquad i = 1, \ldots, n.$$

Finally, (3.12) yields the following explicit formula for the estimated portion $\bar{f}$ of f:

$$\bar{f}(\phi) = -\phi \sum_{i=1}^{n} \bar{h}_i' \left(\bar{\sigma}_i^{-1} \left(\frac{\phi_p}{\phi} \right) \right) \zeta_i(\phi), \quad \frac{\phi_p}{\bar{\sigma}(t_1)} < \phi \le \frac{\phi_p}{\bar{\sigma}(t_N)}. \tag{4.16}$$

4.3. **The quadratic-programming problem.** To the given N data points (4.3) and their transformed values (4.4), we determine the parameters a_i, b_i, c_i and d_i as the unique solution of a least-squares minimization problem with constraints. We define $\boldsymbol{p}_i := (a_i, b_i, c_i, d_i)^{\mathrm{T}}$ and the following vectors:

$$\boldsymbol{p} := \begin{pmatrix} \boldsymbol{p}_1 \\ \boldsymbol{p}_2 \\ \vdots \\ \boldsymbol{p}_n \end{pmatrix}, \quad \boldsymbol{z}_i := \begin{pmatrix} z_{j_i} \\ z_{j_i+1} \\ \vdots \\ z_{j_{i+1}-1} \end{pmatrix}, \quad \boldsymbol{z} := \begin{pmatrix} \boldsymbol{z}_1 \\ \vdots \\ \boldsymbol{z}_n \\ z_N \end{pmatrix}.$$

Then one can write $\bar{s}_i(t) = \boldsymbol{p}_i^{\mathrm{T}}\boldsymbol{q}(t) = \boldsymbol{q}(t)^{\mathrm{T}}\boldsymbol{p}_i$, where $\boldsymbol{q}(t)^{\mathrm{T}} := (t^3, t^2, t, 1)$. Defining also the matrices

$$\boldsymbol{Q}_i := \begin{pmatrix} \boldsymbol{q}(t_{j_i})^{\mathrm{T}} \\ \boldsymbol{q}(t_{j_i+1})^{\mathrm{T}} \\ \vdots \\ \boldsymbol{q}(t_{j_{i+1}-1})^{\mathrm{T}} \end{pmatrix}, \qquad \boldsymbol{Q} := \begin{pmatrix} \boldsymbol{Q}_1 & \boldsymbol{0} & \cdots & \boldsymbol{0} \\ \boldsymbol{0} & \boldsymbol{Q}_2 & & \vdots \\ \vdots & & \ddots & \\ \boldsymbol{0} & \cdots & & \boldsymbol{Q}_n \\ \boldsymbol{0} & \cdots & & \boldsymbol{q}(t_N)^{\mathrm{T}} \end{pmatrix},$$

we can express the objective function J of the minimization problem in the same way as in [8] for the values of z_j instead x_j, namely:

$$J(\boldsymbol{p}) := (\boldsymbol{Q}\boldsymbol{p} - \boldsymbol{z})^{\mathrm{T}}(\boldsymbol{Q}\boldsymbol{p} - \boldsymbol{z}) = \boldsymbol{p}^{\mathrm{T}}\boldsymbol{Q}^{\mathrm{T}}\boldsymbol{Q}\boldsymbol{p} - 2\boldsymbol{z}^{\mathrm{T}}\boldsymbol{Q}\boldsymbol{p} + \boldsymbol{z}^{\mathrm{T}}\boldsymbol{z}. \tag{4.17}$$

We note that the size of $\boldsymbol{Q}$ is $N \times 4n$ and the Hessian of J has the size $4n \times 4n$. To express the equality constraints (4.6)–(4.8) in standard matrix form, we define

$$\boldsymbol{R}_i := \begin{pmatrix} \boldsymbol{q}(t_{j_i})^{\mathrm{T}} \\ \boldsymbol{q}'(t_{j_i})^{\mathrm{T}} \\ \boldsymbol{q}''(t_{j_i})^{\mathrm{T}} \end{pmatrix}, \qquad \boldsymbol{R} := \begin{pmatrix} \boldsymbol{R}_2 & -\boldsymbol{R}_2 & \boldsymbol{0} & \cdots & \boldsymbol{0} \\ \boldsymbol{0} & \boldsymbol{R}_3 & -\boldsymbol{R}_3 & \cdots & \boldsymbol{0} \\ \vdots & & \ddots & \ddots & \vdots \\ \boldsymbol{0} & \cdots & \boldsymbol{0} & \boldsymbol{R}_n & -\boldsymbol{R}_n \end{pmatrix}.$$

Then the equality constraints (4.6)–(4.8) are equivalent to $\boldsymbol{R}_i(\boldsymbol{p}_{i-1} - \boldsymbol{p}_i) = \boldsymbol{0}$ for $i = 2, \ldots, n$, or more compactly, $\boldsymbol{R}\boldsymbol{p} = \boldsymbol{0}$. For the inequality constraints, we let $\varepsilon > 0$ be a small number and $\boldsymbol{1}_{m\times n}$ denote an $m \times n$ matrix full of ones. We define

$$\boldsymbol{e}_1 := \begin{pmatrix} 1 \\ 0 \\ 0 \\ 0 \end{pmatrix}, \qquad \boldsymbol{e}_2 := \begin{pmatrix} 0 \\ 1 \\ 0 \\ 0 \end{pmatrix}, \qquad \boldsymbol{I}_i := \begin{pmatrix} \boldsymbol{e}_i^{\mathrm{T}} & \boldsymbol{0} & \cdots & \boldsymbol{0} \\ \boldsymbol{0} & \boldsymbol{e}_i^{\mathrm{T}} & & \vdots \\ \vdots & & \ddots & \boldsymbol{0} \\ \boldsymbol{0} & \cdots & \boldsymbol{0} & \boldsymbol{e}_i^{\mathrm{T}} \end{pmatrix}_{n\times 4n},$$

$$\boldsymbol{M} := \begin{pmatrix} \boldsymbol{I}_1 \\ -\boldsymbol{I}_2 \\ \begin{pmatrix} \boldsymbol{0}_{1\times 4(n-1)} & \boldsymbol{q}'(t_N)^{\mathrm{T}} \end{pmatrix} \\ \begin{pmatrix} \boldsymbol{0}_{1\times 4(n-1)} & -\boldsymbol{q}''(t_N)^{\mathrm{T}} \end{pmatrix} \end{pmatrix}, \qquad \boldsymbol{b} := -\varepsilon \begin{pmatrix} \boldsymbol{1}_{2n\times 1} \\ 0 \\ 0 \end{pmatrix}$$

Then the inequality constraints $\boldsymbol{M}\boldsymbol{p} \le \boldsymbol{b}$ imply (4.11)–(4.13). For data points (4.4) representing the curved s, the parameters $\boldsymbol{p}$ are determined by the following quadratic programming problem:

$$\begin{aligned} &\text{minimize} && J(\boldsymbol{p}) = (\boldsymbol{Q}\boldsymbol{p} - \boldsymbol{z})^{\mathrm{T}}(\boldsymbol{Q}\boldsymbol{p} - \boldsymbol{z}) \\ &\text{subject to} && \boldsymbol{R}\boldsymbol{p} = \boldsymbol{0}, \quad \boldsymbol{M}\boldsymbol{p} \le \boldsymbol{b}. \end{aligned} \tag{QP}$$

Theorem 4.2. *Given the (transformed) data points* (4.4)*. If the number of data points $N_i = j_{i+1} - j_i$ on each interval $(t_{j_i}, t_{j_{i+1}}]$ satisfies $N_i \ge 4$, then* (QP) *has a unique solution $\boldsymbol{p}$. Moreover, the estimated part of the flux function $\bar{f}$, explicitly given by* (3.12)*, depends continuously on the data points.*

Proof. The uniqueness of the solution of (QP) is obtained by proving that the Hessian $\nabla^2 J = \boldsymbol{Q}^{\mathrm{T}}\boldsymbol{Q}$ is positive definite. To this end, we can consider the calculations in (4.17) with $\boldsymbol{z} = \boldsymbol{0}$ and temporarily let $\boldsymbol{p}$ be an arbitrary vector. Then $\boldsymbol{p}^{\mathrm{T}}\boldsymbol{Q}^{\mathrm{T}}\boldsymbol{Q}\boldsymbol{p} \ge 0$ holds, with equality if and only if

$$\boldsymbol{q}(t_k)^{\mathrm{T}}\boldsymbol{p}_i = 0, \quad k = j_i, \ldots, j_{i+1} - 1, \quad i = 1, \ldots, n, \quad \text{and} \quad \boldsymbol{q}(t_N)^{\mathrm{T}}\boldsymbol{p}_n = 0.$$

Hence, each of the third-order polynomial $\bar{s}_i(t)$ has $N_i \geq 4$ distinct roots t_k which by the fundamental theorem of algebra is possible only if $\boldsymbol{p}_i = 0$. The existence of a solution of (QP) is proved by finding a feasible point of the constraints. A such is given by the following parameters:

$$a_i = -1, \quad b_i = 3t_N, \quad c_i = -3t_N^2, \quad d_i = t_N^3, \quad i = 1, \ldots, n,$$

which correspond to the identical polynomials $\bar{s}_i(t) = (t_N - t)^3$ for all i. They satisfy clearly the constraints (4.11)–(4.13). It is well known (cf. [13, 15]) that the unique minimum $\boldsymbol{p}$ depends continuously on the matrices of (QP), hence on the data points (4.3). □

5. Summaries of the identification methods

We summarize here the two identification methods in the special case $p = 0$, which means that the vessel has a vertex. This case implies that one can identify the end time point of necessary measurements that can be used in the methods; see Theorem 2.2 and Figure 4.

5.1. **Identification of the flux function on parametric form.**

0. Assume that the given data are the initial datum ϕ_0 and the data points (t_j, x_j), $j = 1, \ldots, N$, see (4.3), that represent the shock wave $h(t)$.
1. Fit a function $\bar{h}(t)$ to the data points (t_j, x_j) with any method.
2. Set $\bar{\eta}(t) := \bar{h}(t) - t\bar{h}'(t)$. Then the identified (portion of) flux function is given by the parametrization (3.2), which for $p = 0$ is

$$\big(\phi, \bar{f}(\phi)\big) = \phi_0 \frac{1}{\bar{h}(t)^{1/q}\bar{\eta}(t)}\big(1, -\bar{h}'(t)\big), \quad 0 \leq t \leq t_{2.5}.$$

5.2. **Identification of the flux function as an explicit expression.**

We confine to $q = 1/2$, i.e., a conical vessel. The case for general $q > 0$ is similar; see Section 4.1.

0. Assume that the given data are the initial datum ϕ_0 and the data points (t_j, x_j), $j = 1, \ldots, N$, see (4.3), that represent the shock wave $h(t)$.
1. Transform the data points to $(t_j, z_j) = (t_j, (x_j/2)^3)$, $j = 1, \ldots, N$.
2. Fit the function $\bar{s}(t)$ given by (4.5) of piecewise cubic polynomials $\bar{s}_i(t) = a_i t^3 + b_i t^2 + c_i t + d_i$, $i = 1, \ldots, n$, by solving the optimization problem (QP), where the number of data points N_i in each subinterval should satisfy $N_i \geq 4$.
3. Define $\bar{\sigma}_i^{-1}(t)$ by (4.14) and $\bar{h}_i'(t)$ by (4.15) for $i = 1, \ldots, n$.
4. The identified flux function $\bar{f}(\phi)$ is given by the explicit formula (4.16).

6. Estimation from synthetic and published real data

It is only the part of the upper discontinuity $x = h(t)$, $0 < t < t_{2.5}$, above region I that can be used for the identification of f. In the general case for $p > 0$, it is only possible to detect $t_{2.5}$ when the bottom discontinuity intersects the upper one and there is a jump in the derivative h'. However, in the most common case when the vessel has a vertex, $A(0) = 0$ and $p = 0$ hold. Then Theorem 2.2 implies that $t_{2.5}$ can be detected, either by a jump in the derivative of h', or as the time point after which the solution is stationary. We therefore limit ourselves to the case $p = 0$ and $q = 1/2$, which is a full conical vessel.

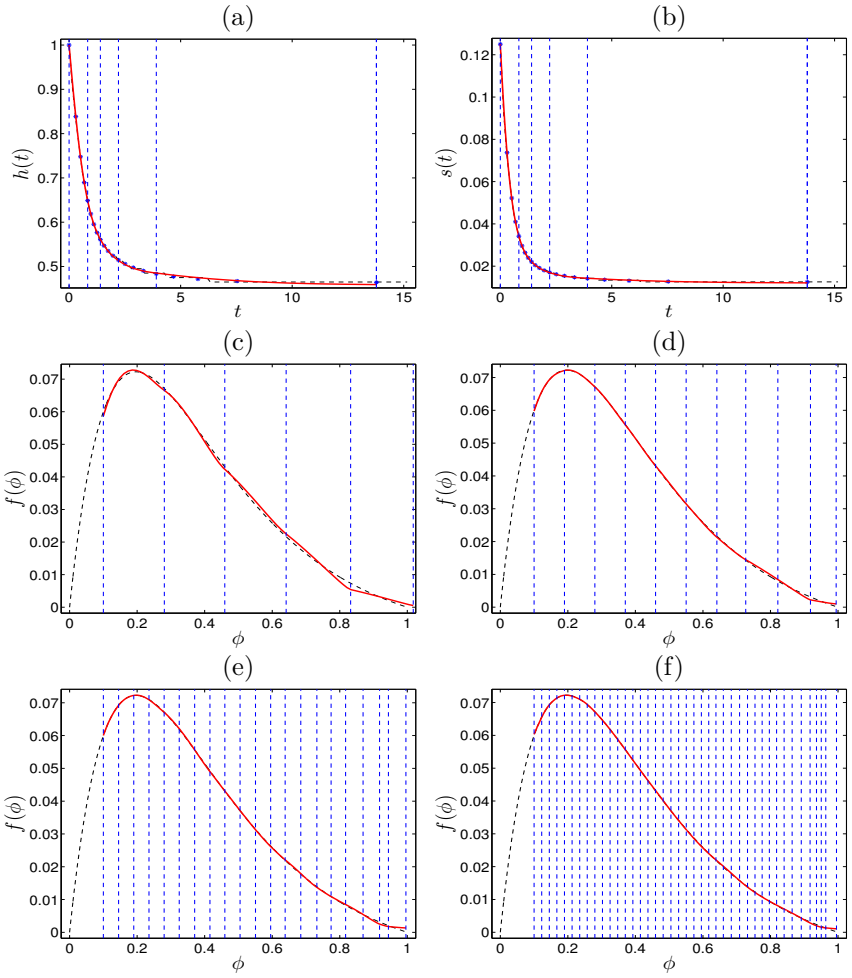

FIGURE 5. Example 1. (a)–(b) Upper discontinuity (dashed black), data points without noise (blue stars) and fitted curve (solid red) obtained with 5 subintervals corresponding to h and s, respectively. (c)–(f) Known flux function (dashed black) and estimated (solid red) for 10, 20 and 40 subintervals, respectively.

6.1. **Example 1.** Synthetic data with hardly any noise are produced by a numerical approximation of the curve $x = h(t)$, $0 \le t \le t_3$, using the Runge-Kutta fourth-order method for the ODEs (2.10)–(2.11), $h(0) = 1$, $\phi_h(0) = \phi_0 = 0.1$, and with the flux function $f(\phi) = \phi(\mathrm{e}^{-5\phi} - \mathrm{e}^{-5})$. To create some examples, we use different number of data points from the approximate ODE solution h_{ODE}, namely $(x_j, t_j) = (h_{\mathrm{ODE}}(t_j), t_j)$, $j = 1, \ldots, N$, where $N-1$ is divisible by 4 and $(N-1)/4$ is the number of subintervals. The N data points have been chosen (almost) equidistantly along the ϕ-axis by using the injective relation to time given by the first component of (3.8). Figure 5 shows the results of the identification procedure of Section 5.2 with an explicit flux function. With 5 subintervals, plots (a) and (b) show the data points and the fitted curves $\bar{h}$ and $\bar{s}$, where the coefficients of $\bar{s}$

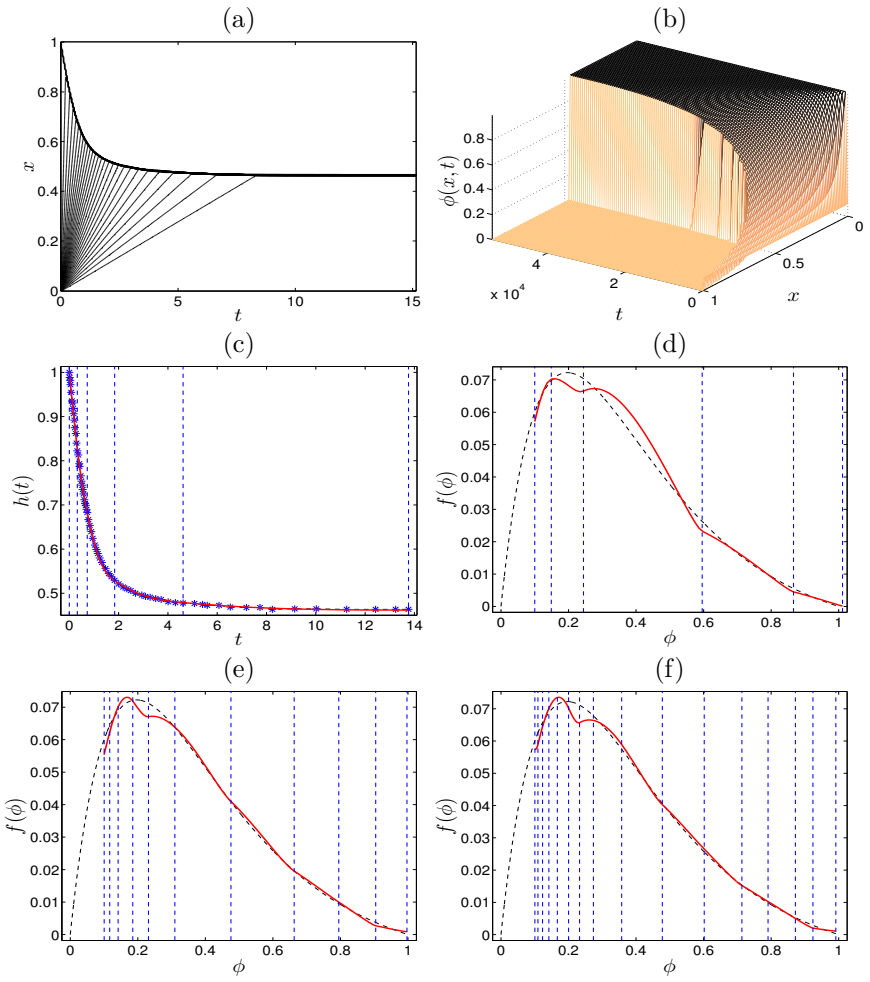

FIGURE 6. Example 2. (a) Isoconcentration curves of a numerical solution of (1.2a)–(1.2c) shown in (b) obtained with a Godunov approximation. (c) Data points (blue stars) and resulting h-curve of the optimization for $n = 5$ subintervals (solid red). (d)–(f) Known flux function (dashed black) and identified (solid red) for 5, 10 and 15 subintervals, respectively.

are obtained as the solution of the quadratic programming problem (QP). The identified flux function, together with the known one, is plotted in (c). The same procedure gives the identified fluxes shown in (d)–(f) for 10, 20 and 40 subintervals. The more subintervals, and larger N, the visually better is the identification of f; however, there are several inflection points created, at least for low N. Apart from these inflection points, the flux function is identified and we conclude that the identification procedure with cubic splines works.

6.2. **Example 2.** With the same flux function as in Example 1, we produce synthetic data by means of a numerical solution of the direct problem (1.2) by using

a finite difference scheme with Godunov's numerical flux; cf. [7]. The numerical solution is obtained with a division of the vessel height into 100 spatial cells; see Figure 6 (a) and (b). The upper discontinuity is then approximated by a piecewise affine function interpolating 103 data points chosen at the uppermost spatial cell such that $\phi \geq 0.9\phi_0 = 0.09$. From the interpolating curve, $4n + 1 = 21$ data points are taken for the identification procedure with $n = 5$ subintervals. The identification procedure of Section 5.2 is used. The optimization procedure of Section 4 results in the h-curve shown in (c). The identified fluxes are shown in plots (d)–(f) for 5, 10 and 15 subintervals, respectively.

In this example, the identification of the flux function does not improve much with the number of data points N used. It seems that the errors in the synthetic data are either smoothed out or amplified at different locations of the flux curve. For small times, the curve $x = h(t)$ declines fast and the corresponding ϕ-values just below the interface lie near the maximum point of f. Unfortunately, the relatively small errors in data are amplified resulting in the oscillations near the maximum point shown in Figure 6 (d)–(f).

6.3. **Example 3.** We use the experimental data of White and Verdone [45, Figure 11], who measured the height of the supernatant-suspension discontinuity during the settling of magnesium hydroxide $Mg(OH)_2$ in water. Three tests with different concentrations were reported in partly a cylindrical vessel and partly a full cone; see Figure 7 (a). The density of $Mg(OH)_2$ is $\varrho_s = 2344.6\,\mathrm{kg/m^3}$, so the three initial concentrations $C_0 = 50$, 60 and $70\,\mathrm{g/l}$ correspond to the volume fractions $\phi_0 = C_0/\varrho_s = 0.0213$, 0.0256 and 0.0299, respectively. Unfortunately, the experiments were not performed to steady state. Our identification procedure applied to three data sets of the cone, working with dimensional variables, yields three slightly different estimated parts of flux functions to which one can fit a final single flux function. The latter can then be used for numerical simulation (as in Example 2) which can be compared to the results of the three experiments made in the cylindrical vessel.

It turns out that the parametric formula (3.2) yields closer estimations of the three cone data sets. To each data set we fit the decreasing and strictly convex function

$$\bar{h}(t) = \frac{a}{t+b} + ct + d.$$

For example, the data for $C_0 = 50\,\mathrm{g/l}$ gave the coefficients $a = 0.7621$, $b = 1.2984$, $c = 0.02146$ and $d = 0.4111$. The resulted three h-curves are shown in Figure 7 (b). Plot (c) shows the estimated three parts of flux functions with the parametric formulas (3.2). To these three curves, we fitted a final flux of the form

$$\tilde{f}(C) = \frac{\mathrm{e}^{1-C/\varrho_s} - 1}{\mathrm{e} - 1} \frac{v_0 C}{1 + (C/\bar{C})^n} \tag{6.1}$$

with the parameters $v_0 = 3.5784 \times 10^{-4}\,\mathrm{m/s}$, $\bar{C} = 49.570\,\mathrm{g/l}$ and $n = 2.6227$. This flux function satisfies $\tilde{f}(0) = \tilde{f}(\varrho_s) = 0$ and is used for the numerical simulation of batch settling in a cylindrical vessel with the three initial concentrations $C_0 = 50$, 60 and $70\,\mathrm{g/l}$. The simulation results are plotted in Figure 7 (d)–(f) together with the corresponding cylindrical data. Initially, the agreements between the simulations and the data are good. The differences seen for later times have probably several causes, such as sensitive identification method, non-complete data sets, polydisperse

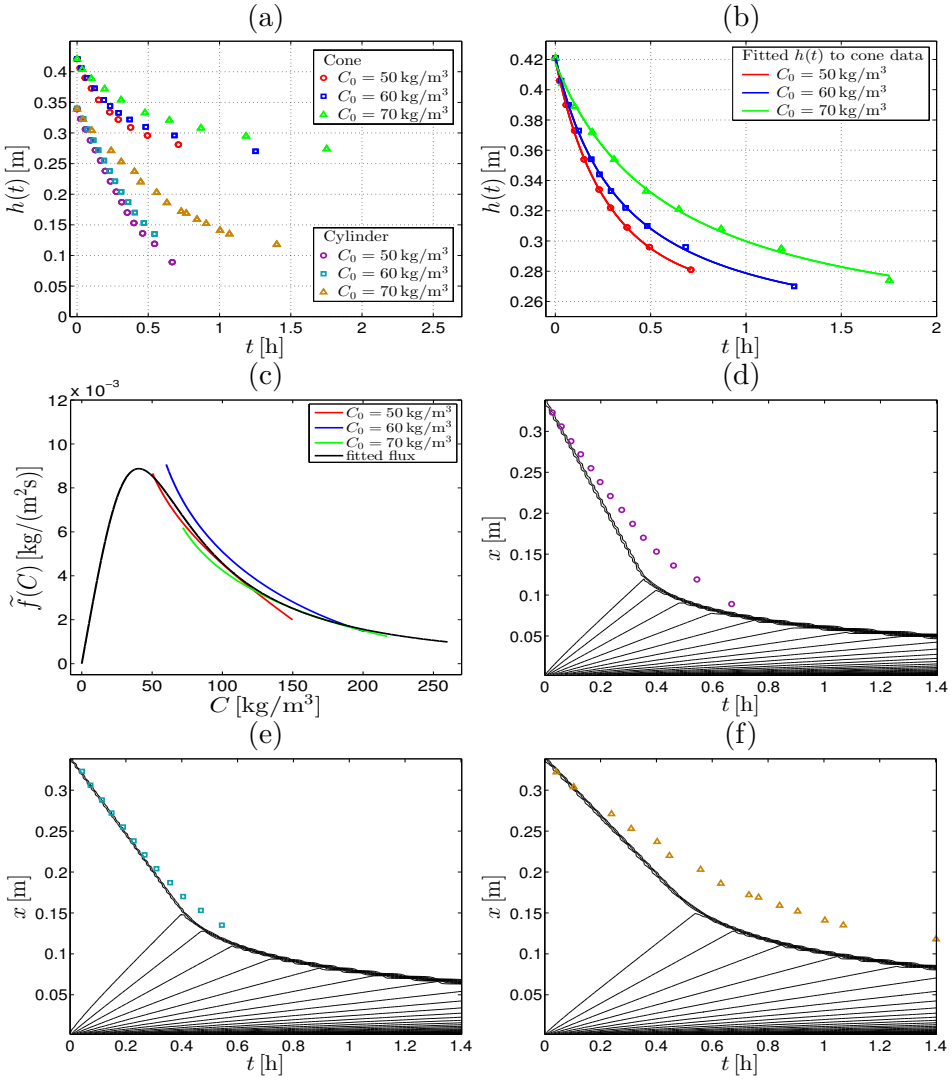

FIGURE 7. (a) Experimental data of sedimentation of $Mg(OH)_2$ in water in a conical and cylindrical vessel; from White and Verdone [45, Figure 11]. (b) Fitted h-curves to cone data. (c) Identified portions of flux function for each data set (coloured) and fitted flux function $\tilde{f}(C)$ (6.1). (d)–(f) Simulated batch tests in cylindrical vessel with $\tilde{f}(C)$ and cylinder data points from (a).

sedimentation (certain width of the size distribution of particles) and compressive effects at higher concentrations.

7. Conclusions

A new identification method for the flux function of hindered settling of particles in a liquid has been presented. The initial homogeneous concentration ϕ_0 and

detailed measurements of the declining supernatant-suspension discontinuity $x = h(t)$ are the inputs for the inverse problem (IP) of identifying the nonlinear flux function of the scalar hyperbolic problem (1.2). The solution of (IP) is found by utilizing the constructed solutions of (1.2) by the method of characteristics for hyperbolic PDEs in qualitatively different cases. The solution of (IP) is presented in two version in Theorems 3.1 (parametric) and 3.2 (explicit expression).

Another new result of this work is Theorem 2.2, which states the unique entropy solution of the direct problem (1.2) in the case of a vessel with a vertex at the bottom. A full cone is the most common type of vessel with varying cross-sectional are used in industry for batch sedimentation tests. In addition, this is of particular advantage for (IP), since the end time point of data collection can then be detected from only observing the shock wave $x = h(t)$ (see Section 2.3).

Theoretically, only one batch experiment is needed and almost the entire flux function can be identified, namely for the interval $[\phi_0, \phi_{\max}]$. The identified flux function $\bar{f}$ can be represented accurately with parametric formulas after fitting of a function $\bar{h}(t)$ to data (Theorem 3.1). As an appealing alternative, $\bar{f}$ can be expressed by an explicit function (Theorem 3.2); however, the method is slightly less flexible, since the function fitted to transformed data $\bar{s}(t)$ is limited to certain expressions, each leading to a transformed function $\bar{\sigma}(t)$ having an explicit inverse. Fortunately, a function $\bar{s}(t)$ consisting of piecewise cubic polynomials is possible. Application of the method, which includes the optimization problem of Section 4, to synthetic data (i.e., produced by a known flux) with hardly any noise demonstrates it success (Section 6). However, larger errors of the data imply that the method to identify an explicit flux function introduces several inflection points of the identified flux function, despite this only has one such (for synthetic data). From the limited real data sets from literature, we found that the parametric formulas for the flux function (Theorem 3.1) gave better results, which we present in Section 6.3.

The huge interest in flux identification that has lead to the previous methods referred to in Section 1.2 are all confined to cylindrical vessels. The advantages of the presented method are that only one experiment is needed and that this experiment is easy to perform. Previous methods (cylindrical vessels) are either easy to perform (standard batch test), resulting at the best to one point below the inflection point ϕ_{infl} of the flux curve and a subinterval of $[\phi_{\text{infl}}, \phi_{\max}]$; or difficult to perform and require special equipment (batch test with high concentration on top of clear liquid), but can estimate some of the concave part of the flux [4, 8, 18]. The advantages of these previous methods are that the concavity/convexity of the flux function below/above the inflection point is naturally built into those identification methods, which also preserve the C^2 regularity of the function fitted to data over to the identified flux $\bar{f}$. The new method satisfies only $\bar{s} \in C^2 \Rightarrow \bar{f} \in C^1$ (Theorem 4.1). Further development of the new method to account for convexity preservation is needed. Other shortcomings of the presented method is that it relies on a one-dimensional model, taking no wall effects into account (except for the varying cross-sectional area).

Acknowledgement

RB is supported by Fondecyt project 1130154; BASAL project CMM, Universidad de Chile and Centro de Investigación en Ingeniería Matemática (CI^{2}MA),

Universidad de Concepción; Fondef project ID15I10291; and CRHIAM, project CONICYT/FONDAP/15130015.

References

[1] G. Anestis. *Eine eindimensionale Theorie der Sedimentation in Absetzbehältern veränderlichen Querschnitts und in Zentrifugen*. PhD thesis, TU Vienna, Austria, 1981.

[2] D. P. Ballou. Solutions to nonlinear hyperbolic Cauchy problems without convexity conditions. *Trans. Amer. Math. Soc.*, 152:441–460, 1970.

[3] S. Berres, R. Bürger, A. Coronel, and M. Sepulveda. Numerical identification of parameters for a flocculated suspension from concentration measurements during batch centrifugation. *Chem. Eng. J.*, 111:91–103, 2005.

[4] F. Betancourt, R. Bürger, S. Diehl, and C. Mejías. Advanced methods of flux identification for clarifier–thickener simulation models. *Minerals Eng.*, 63:2–15, 2014.

[5] U. Borgmann and W. P. Norwood. Sediment toxicity testing using large water–sediment ratios: an alternative to water renewal. *Environm. Pollution*, 106(3):333–339, 1999.

[6] R. Bürger, J. Careaga, and S. Diehl. Entropy solutions of a scalar conservation law modelling sedimentation in vessels with varying cross-sectional area. Preprint 2016-21, Centro de Investigación en Ingeniería Matemática, Universidad de Concepción, 2016. Submitted.

[7] R. Bürger, J. J. R. Damasceno, and K. H. Karlsen. A mathematical model for batch and continuous thickening of flocculated suspensions in vessels with varying cross-section. *Int. J. Miner. Process.*, 73:183–208, 2004.

[8] R. Bürger and S. Diehl. Convexity-preserving flux identification for scalar conservation laws modelling sedimentation. *Inverse Problems*, 29(4):045008, 2013.

[9] C. Castro and E. Zuazua. Flux identification for 1-d scalar conservation laws in the presence of shocks. *Math. Comp.*, 80(276):2025–2070, 2011.

[10] K.-S. Cheng. Constructing solutions of a single conservation law. *J. Differ. Equat.*, 49:344–358, 1983.

[11] Y.-T. Choi, L. Xie, and N. M. Wereley. Testing and analysis of magnetorheological fluid sedimentation in a column using a vertical axis inductance monitoring system. *Smart Mater. Struct.*, 25(4):04LT01, 2016.

[12] A. Coronel, F. James, and M. Sepúlveda. Numerical identification of parameters for a model of sedimentation processes. *Inverse Probl.*, 19(4):951–972, 2003.

[13] J. W. Daniel. Stability of the solution of definite quadratic programs. *Mathematical Programming*, 5:41–53, 1973.

[14] P. J. T. Dankers and J. C. Winterwerp. Hindered settling of mud flocs: Theory and validation. *Continent. Shelf Res.*, 27(14):1893–1907, 2007.

[15] G. B. Dantzig, J. Folkman, and N. Shapiro. On the continuity of the minimum set of a continuous function. *J. Math. Anal. Appl.*, 17(3):519–548, 1967.

[16] J. De Clercq, M. Devisscher, I. Boonen, J. Defrancq, and P. A. Vanrolleghem. Analysis and simulation of the sludge profile dynamics in a full-scale clarifier. *J. Chem. Tech. Biotechnol.*, 80(5):523–530, 2005.

[17] J. De Clercq, F. Jacobs, D. J. Kinnear, I. Nopens, R. A. Dierckx, J. Defrancq, and P. A. Vanrolleghem. Detailed spatio-temporal solids concentration profiling during batch settling of activated sludge using a radiotracer. *Water Res.*, 39:2125–2135, 2005.

[18] S. Diehl. Estimation of the batch-settling flux function for an ideal suspension from only two experiments. *Chem. Eng. Sci.*, 62:4589–4601, 2007.

[19] S. Diehl. Operating charts for continuous sedimentation IV: Limitations for control of dynamic behaviour. *J. Eng. Math.*, 60:249–264, 2008.

[20] S. Diehl. A regulator for continuous sedimentation in ideal clarifier-thickener units. *J. Eng. Math.*, 60:265–291, 2008.

[21] S. Diehl. Numerical identification of constitutive functions in scalar nonlinear convection–diffusion equations with application to batch sedimentation. *Appl. Num. Math.*, 95:154–172, 2015.

[22] S. Diehl and S. Farås. Control of an ideal activated sludge process in wastewater treatment via an ODE-PDE model. *J. Process Control*, 23(3):359–381, 2013.

[23] E. M. Fernández-Berdaguer and G. B. Savioli. An inverse problem arising from the displacement of oil by water in porous media. *Appl. Num. Math.*, 59(10):2452–2466, 2009.

[24] C. Grima-Olmedo, J. A. Butragueño-Muñoz, Á. Ramírez-Gómez, and D. G.-L. Galindo. Review of equipment for mine waste: From the conventional thickener to the deep cone for paste production. *DYNA (Bilbao)*, 2012.
[25] L. Hernando, A. Omari, and D. Reungoat. Experimental study of sedimentation of concentrated mono-disperse suspensions: Determination of sedimentation modes. *Powder Tech.*, 258:265–271, 2014.
[26] H. Holden, F. S. Priuli, and N. H. Risebro. On an inverse problem for scalar conservation laws. *Inverse Problems*, 30(3), 2014.
[27] H. Holden and N. H. Risebro. *Front Tracking for Hyperbolic Conservation Laws*. Second Edition, Springer Verlag, Berlin, 2015.
[28] E. Iritani, T. Hashimoto, and N. Katagiri. Gravity consolidation-sedimentation behaviors of concentrated TiO_2 suspension. *Chem. Eng. Sci.*, 64(21):4414–4423, 2009.
[29] F. James and M. Sepúlveda. Convergence results for the flux identification in a scalar conservation law. *SIAM J. Control Optim.*, 37(3):869–891, 1999.
[30] H. Jiao, A. Wu, H. Wang, S. Zhong, R. Ruan, and S. Yin. The solids concentration distribution in the deep cone thickener: A pilot scale test. *Korean J. Chem. Eng.*, 30(2):262–268, 2013.
[31] M. Johnson, J. Peakall, M. Fairweather, S. Biggs, D. Harbottle, and T. N. Hunter. Characterization of multiple hindered settling regimes in aggregated mineral suspensions. *Ind. Eng. Chem. Res.*, 55(37):9983–9993, 2016.
[32] H. Kang and K. Tanuma. Inverse problems for scalar conservation laws. *Inverse Problems*, 21(3):1047–1059, 2005.
[33] R. D. Karamisheva and M. A. Islam. Development of a new model for batch sedimentation and application to secondary settling tanks design. *Water Environ. Res.*, 7:3066–3073, 2005.
[34] G. J. Kynch. A theory of sedimentation. *Trans. Faraday Soc.*, 48:166–176, 1952.
[35] Z. Li and D. Zhang. A model for characterizing the process of activated sludge compression settling. *Advanced Materials Res.*, 518–523:3680–3686, 2012.
[36] W. A. S. K. Mancell-Egala, D. J. Kinnear, K. L. Jones, H. De Clippeleir, I. Takács, and S. N. Murthy. Limit of stokesian settling concentration characterizes sludge settling velocity. *Water Res.*, 90:100–110, 2016.
[37] M. Marsi and V. P. Evangelou. Chemical and physical behavior of two Kentucky soils: III. saturated hydraulic conductivity – Imhoff cone test relationships. *J. Environm. Sci. Health. Part A: Environm. Sci. Eng. Toxicology*, 26(7):1195–1215, 1991.
[38] J. Martin, N. Rakotomalala, and D. Salin. Accurate determination of the sedimentation flux of concentrated suspensions. *Phys. Fluids*, 7(10):2510–2512, 1995.
[39] O. A. Oleinik. Uniqueness and stability of the generalized solution of the Cauchy problem for a quasi-linear equation. *Uspekhi Mat. Nauk*, 14:165–170, 1959. Amer. Math. Soc. Trans. Ser. 2, 33, (1964), pp. 285–290.
[40] J. B. K. Park, R. J. Craggs, and A. N. Shilton. Recycling algae to improve species control and harvest efficiency from a high rate algal pond. *Water Res.*, 45(20):6637–6649, 2011.
[41] V. Prigiobbe, S. Ko, C. Huh, and S. L. Bryant. Measuring and modeling the magnetic settling of superparamagnetic nanoparticle dispersions. *J. Colloid Interface Sci.*, 447:58–67, 2015.
[42] G. B. Savioli and E. M. Fernández-Berdaguer. The estimation of oil water displacement functions. *Latin American Applied Res.*, 37(3):187–194, 2007.
[43] R. E. Sojka, D. L. Carter, and M. J. Brown. Imhoff cone determination of sediment in irrigation runoff. *Soil Science Society of America Journal*, 56(3):884–890, 1992.
[44] N. Stepova and Yu. I. Kalugin. Mathematical modeling of a secondary clarifier with cone-shaped bottom. *Int. J. Fluid Mech. Res.*, 38(5):458–478, 2011.
[45] D. A. White and N. Verdone. Numerical modelling of sedimentation processes. *Chem. Eng. Sci.*, 55:2213–2222, 2000.
[46] J. Zhang, X. Yin, and J. Liu. Economic MPC of deep cone thickeners in coal beneficiation. *Can. J. Chem. Eng.*, 94(3):498–505, 2016.